ISSN: 2710-0588

Numerical Study on The Effects of Inclination and Fracture Length on The Strength and Damage Evolution of Orthogonally Fractured Sandstone

Liming Yang

School of Civil Engineering, Henan Polytechnic University, Jiaozuo 454003, Henan, China

Abstract

Cross fractures are commonly found in natural rock masses and typically exhibit primary and secondary classifications, with their geometric characteristics significantly influencing the stability of rock engineering. This study calibrates the mesoscopic parameters of PFC2D through sandstone laboratory tests and systematically investigates the effects of orthogonal fracture inclination angle and primary and secondary fracture lengths on the mechanical properties and damage evolution of sandstone. The results indicate that the peak stress and peak strain initially decrease and subsequently increase in a concave pattern as the inclination angle rises, reaching a minimum value at an angle of 60°. At an inclination angle of 0°, an increase in the secondary fracture length causes the fracture initiation location to shift from around the orthogonal fractures to the tips of the primary fractures, resulting in a change in the failure mode from diagonal failure to a "figure-eight" shape caused by secondary fracture penetration. When the inclination angle is between 30° and 60°, cracks preferentially initiate at the tips of the primary fractures, and the failure mode gradually transitions from secondary crack propagation to primary crack penetration. At an inclination angle of 90°, cracks at the tips of the secondary fractures initiate first; however, the final failure characteristic exhibits the "figure-eight" shape of primary fracture penetration. Further analysis reveals that the samples mainly experience tensile failure, with cracks propagating from the prefabricated fractures and extending outward in the direction of the principal stress. The findings provide a theoretical basis for the stability assessment of fractured rock masses.

Keywords

Sandstone; Orthogonal fractures; Numerical analysis; Damage evolution; Failure mode.

1. Introduction

The rock mass is a discontinuous medium formed by complex geological processes, typically characterized by multiple sets of intersecting fractures, with a significant distinction between primary and secondary fractures. The spatial distribution, geometric morphology, and propagation characteristics of these fractures directly influence the mechanical behavior and failure patterns of the rock mass, which critically affect the stability of major engineering projects such as hydropower, transportation tunnels, and mining operations, even posing threats to engineering safety. Therefore, it is of great engineering significance to conduct in-depth research on the mechanical properties and damage evolution mechanisms of intersecting fracture rock masses.

Numerous studies have shown that the presence of fractures greatly impacts the mechanical and damage failure characteristics of rock masses. For instance, Yang S [1], Huimei Z [2], and others have explored the mechanical properties of rock masses and the propagation patterns of fractures through pre-fabricated fractures. Li C [3] fabricated rock masses with fractures at

ISSN: 2710-0588

different dip angles to study the propagation of internal fractures. Guangfeng L [4] found that the length of cracks significantly affects the strength and deformation characteristics of unanchored samples. Haeri H [5] analyzed the effects of pre-fabricated cracks at different angles under uniaxial compression on rock stress, strain, and strength, and examined the fracture process of specimens. These studies effectively investigated the initiation and propagation of cracks within rock masses; however, fractures typically appear in groups in natural rock masses. Thus, studying the mechanical properties of rock masses containing multiple fractures is of considerable importance for understanding the performance of actual rock masses.

Ma W [6] studied the cracking behavior and failure process of rock masses through two disconnected pre-fabricated cracks. Du X [7] set up multiple cracks to analyze the impact of different quantities of fractures on rock mass strength. Peng C [8] pre-fabricated Y-shaped fractures and analyzed the effects of different angles of pre-fabricated Y-shaped fractures on the mechanical strength characteristics and cracking evolution of rock masses. Lin H [9] created a soft-hard composite rock with three parallel fractures and conducted uniaxial compression tests to analyze the influences of fracture angles and widths on crack propagation behavior. Chen Q [10] fabricated specimens containing parallel joint groups with different dip angles to simulate natural rock masses and performed shear tests on the specimens under various normal stresses to study the effects of normal stress and fracture dip angle on the strength and failure characteristics of such rock masses. The results indicated that the cracking pattern observed in samples containing multiple fractures was similar to that in rock masses with two fractures. These studies also showed that mechanical properties and damage failure characteristics are closely related to the number and shape of fractures.

Due to the challenges associated with pre-fabricated fractures, researchers both domestically and internationally have conducted studies on the mechanical properties and damage failure characteristics of fractured rock masses, often employing numerical simulation methods. For example, Castro-Filgueira U [11] and colleagues established numerical models using the PFC numerical simulation software and simulated compression tests, revealing a high degree of correlation in mechanical properties between their results and laboratory experiments. Zhao C [12] applied the discrete element method to comparatively analyze the cracking behavior of rocks under uniaxial and biaxial compression and the influence of confining pressure on tensile and shear behavior. Lee H [13] simulated the initiation and propagation of cracks in three types of rock materials, summarizing the similarities and differences based on material variations. Bahaaddini M [14] and Fan X [15] investigated the effects of fracture direction, length, and joint mechanical properties on the strength and failure behavior of rock masses in three-dimensional space. Wu J [16] studied the effects of different lengths of pre-fabricated cracks and varying confining pressures on the dilatancy characteristics and acoustic emission of rocks. Feng P [17] analyzed the impact of different loading rates on the fracture process of pre-fabricated cracked rocks, while Yang X [18] used the PFC3D program to examine the influence of fracture direction on rock mass strength.

Current research primarily focuses on the macroscopic mechanical responses and ultimate failure modes of fractured rock masses, while there is a lack of systematic studies on the micro-damage evolution processes, especially concerning the differential propagation behaviors of primary and secondary fractures. To address this, this study will concentrate on exploring the crack initiation mechanisms and dynamic propagation laws of orthogonal fractured rock masses during uniaxial compression.

ISSN: 2710-0588

2. Basic Theory and Sample Model

2.1. Basic theory

This study utilizes the two-dimensional version of the Particle Flow Code (PFC2D) developed by Itasca, USA, for numerical simulations. PFC is a discrete element method (DEM) software based on the micromechanics of discontinuous media theory, which focuses on simulating the interactions of rigid particle assemblies to reveal the mechanical behavior of materials. The program abstracts the research subject as a bulk material or a bonded material system, providing various embedded contact models such as linear, parallel bond, and smooth joint models. The macroscopic mechanical properties of the medium are determined by the geometric attributes of the particles and micro-mechanical parameters.

At the micromechanical level, PFC characterizes contact forces by allowing controlled overlapping between particles, with mechanical evolution strictly following Newton's second law. The failure modes of bonding between particles include both shear and tensile forms. The macroscopic mechanical response of the medium essentially reflects the dynamic evolution of the particle contact network and bonding state at the microscopic scale. This feature enables PFC to naturally simulate the initiation and propagation of cracks in solid materials such as rock masses, as well as the deformation, flow, and instability failure processes of particle assemblies. In this study, to more accurately reflect the initiation and propagation evolution of cracks in fractured rock masses, a parallel bond model was adopted (Figure 1), allowing for the simulation analysis by controlling the micro-mechanical parameters of the particles and the bonds.

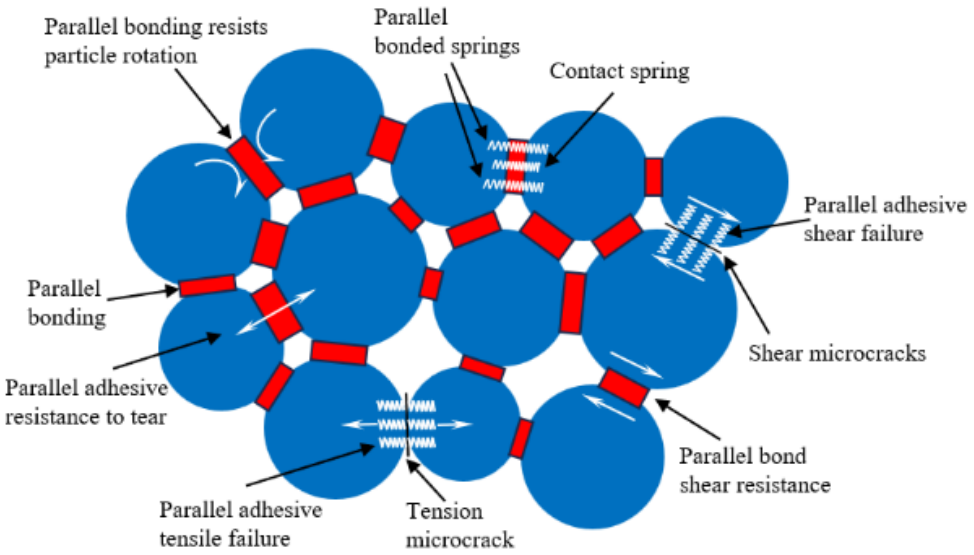

Figure 1. Schematic diagram of parallel bonding model

2.2. Calibration parameters

Micro-mechanical parameters were calibrated using a trial-and-error method, by continuously adjusting parameters such as tensile strength, cohesion, and internal friction angle until the simulated stress-strain curves closely matched those of the sandstone specimens. The resulting micro-mechanical parameters are shown in Table 1. The laboratory experiments are depicted in Figure 2. As seen in Figure 3, there is little difference in the peak strengths and peak strains between the numerical simulation curves and the sandstone specimen curves, indicating that the parameter settings in PFC2D are largely reasonable.

ISSN: 2710-0588

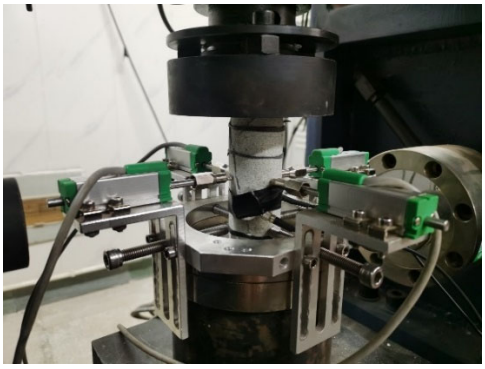

Figure 2. Indoor test

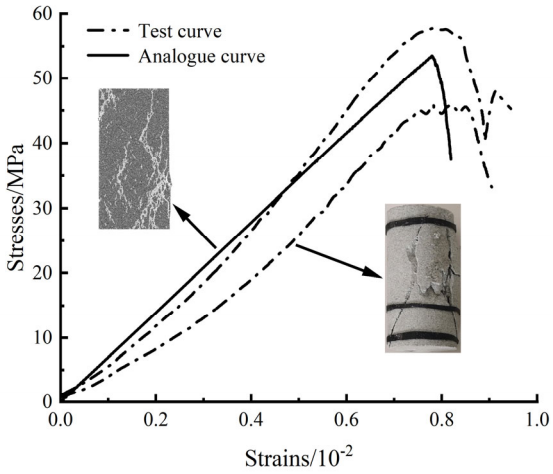

Figure 3. Stress-strain curve

Table 1. Micro mechanical parameters

Type	Microscopic parameters	numerical value
Basic particle parameters	Minimum particle size D_{min}/mm	0.25
	Maximum particle size D_{max}/mm	0.41
	Particle contact modulus E_c/GPa	3.5
	Particle contact stiffness k_m/k_n	2
	Friction coefficient μ	0.6
Parallel bond parameter	Parallel bond modulus E_c/GPa	3.5
	Normal tangent stiffness k_n/k_s	2
	Internal friction angle φ/(°)	38
	Tensile strength σ/MPa	23
	Bond strength C/MPa	17

2.3. Simulation scheme

After calibrating the parameters using the trial-and-error method, uniaxial compression numerical simulations were conducted on different models. The simulation was halted when the stress dropped to 60% of the peak stress strength. A comparative analysis was performed on the simulation results for different inclination angles and lengths of primary and secondary fractures, observing the effects of fracture inclination and primary and secondary fracture lengths on the initiation and propagation evolution of cracks in the rock mass.

The numerical simulation model dimensions in this study were 50mm × 100mm, with the angle α between the prefabricated primary fracture and the principal stress direction set at 0°, 30°, 60°, and 90°. The angle between the primary and secondary fractures was uniformly 90°, with

ISSN: 2710-0588

the lengths of the primary fractures m being 10mm and 20mm, and the lengths of the secondary fractures n being 5mm, 10mm, and 15mm. The specimen numbers are listed in Table 2.

Table 2. Sample Numbers

α/(°)	10/mm 5/mm	20/mm 5/mm	20/mm 10/mm	20/mm 15/mm
0	0-10-5	0-20-5	0-20-10	0-20-15
30	30-10-5	30-20-5	30-20-10	30-20-15
60	60-10-5	60-20-5	60-20-10	60-20-15
90	90-10-5	90-20-5	90-20-10	90-20-15

3. Mechanical Properties

3.1. Influence of fracture inclination on mechanical properties

The angles of the fractures described below all refer to the angle α between the main fracture and the principal stress direction. Axial compression simulation tests were conducted on various numerical models in Table 2, and the resulting stress-strain curves are shown in Figure 4. From Figure 4, it can be observed that as the fracture angle increases, the peak stress and peak strain of each specimen show a trend of first decreasing and then increasing. For specimens with fracture angles between 0° and 60°, both the peak stress and peak strain decrease as the angle increases; however, for those between 60° and 90°, these values tend to increase with the angle. Notably, within the range of fracture angles from 0° to 30°, the peak stress and peak strain of the 20-5 specimen show the greatest reductions, whereas the 20-10 specimen exhibits the smallest reduction in peak stress, with a slight increase in peak strain. This indicates that the 20-5 specimen is more sensitive to changes in angle within the 0° to 30° range.

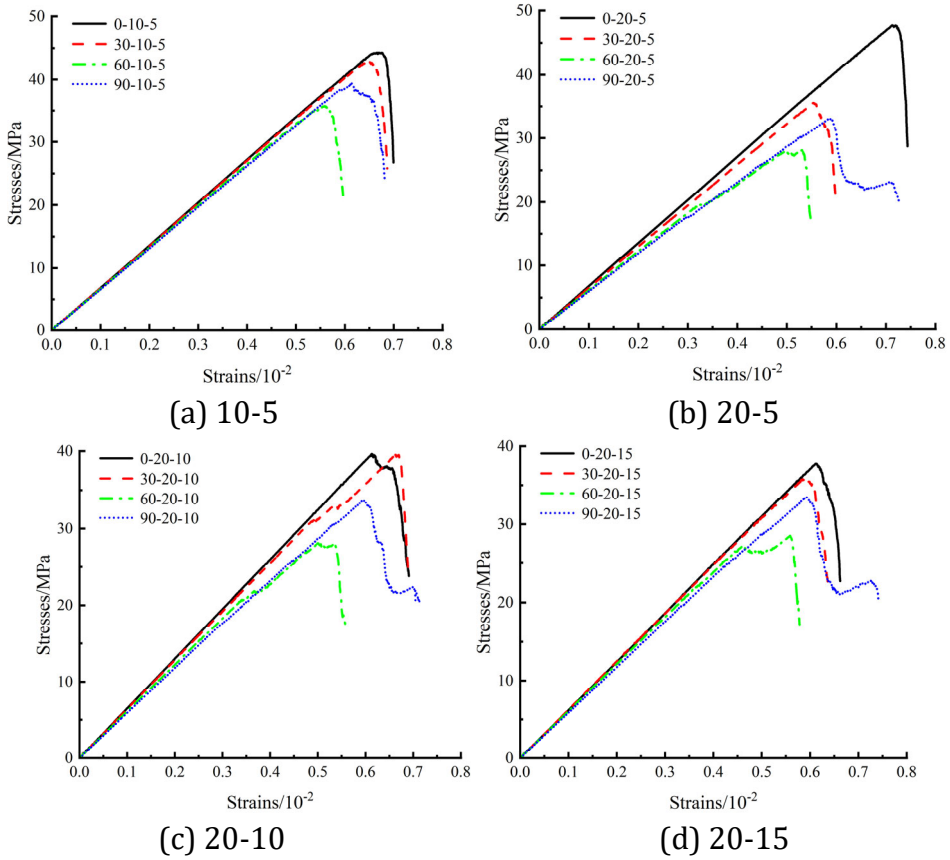

Figure 4. Stress-strain curves for different inclination angles

ISSN: 2710-0588

To observe the variation of peak stress and peak strain with fracture angle more clearly, the peak stress and peak strain under different fracture angles from Figure 4 are plotted in Figure 5. From Figure 5(a), it is evident that within the fracture angle range of 0° to 30°, the peak stress of the 20-5 specimen exhibits the largest reduction, at 25.50%, while the 20-10 specimen shows the smallest reduction, merely 0.29%. In the range of 30° to 60°, the 20-10 specimen also experiences the greatest reduction in peak stress, at 28.83%, while the 10-5 specimen shows the smallest reduction at 16.70%. Overall, the reduction in peak stress in the 30° to 60° range is greater than that in the 0° to 30° range. Figure 5(b) indicates that within the 0° to 30° range, only the peak strain of the 20-10 specimen exhibits an increasing trend, while all other specimens show a decreasing trend, with the 20-5 specimen demonstrating the largest reduction at 22.44%. For the 30° to 60° range, the 20-10 specimen has the largest reduction in peak strain, at 24.43%. In the 60° to 90° range, all specimens exhibit an increasing trend in peak stress and peak strain. Overall, the peak stress and peak strain of the specimens show a "concave" variation trend with changes in fracture angle, attaining their minimum values at a fracture angle of 60°.

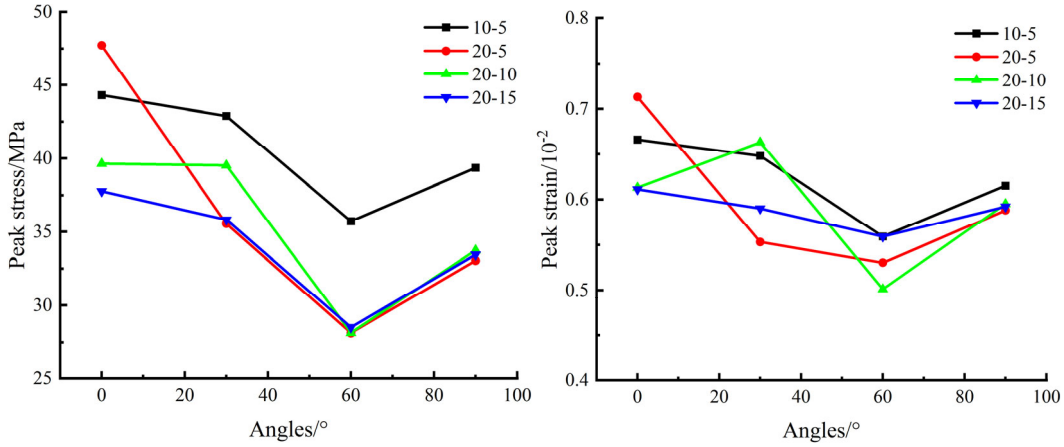

(a) Peak stress (b) Peak strain

Figure 5. Peak stress, peak strain variation curve with inclination angles

3.2. The influence of the length difference between primary and secondary fractures on mechanical properties

The comparative stress-strain curves under different fracture lengths are illustrated in Figure 6. As seen in Figure 6, for the specimen with a fracture angle of 0°, when the length of the secondary fracture remains constant, the peak stress increases with the increase in the length of the main fracture; conversely, when the length of the main fracture is constant, the peak stress decreases with the increase in the length of the secondary fracture. For the specimen with a fracture angle of 30°, when the length of the secondary fracture is constant, the peak stress decreases with an increase in the main fracture length; and when the main fracture length is constant, the peak stress first increases and then decreases as the length of the secondary fracture increases, overall presenting an increasing trend. For specimens with fracture angles of 60° and 90°, with a constant secondary fracture length, the peak stress decreases with an increase in the main fracture length; whereas when the main fracture length remains constant, the peak stress remains relatively unchanged with an increase in the secondary fracture length.

ISSN: 2710-0588

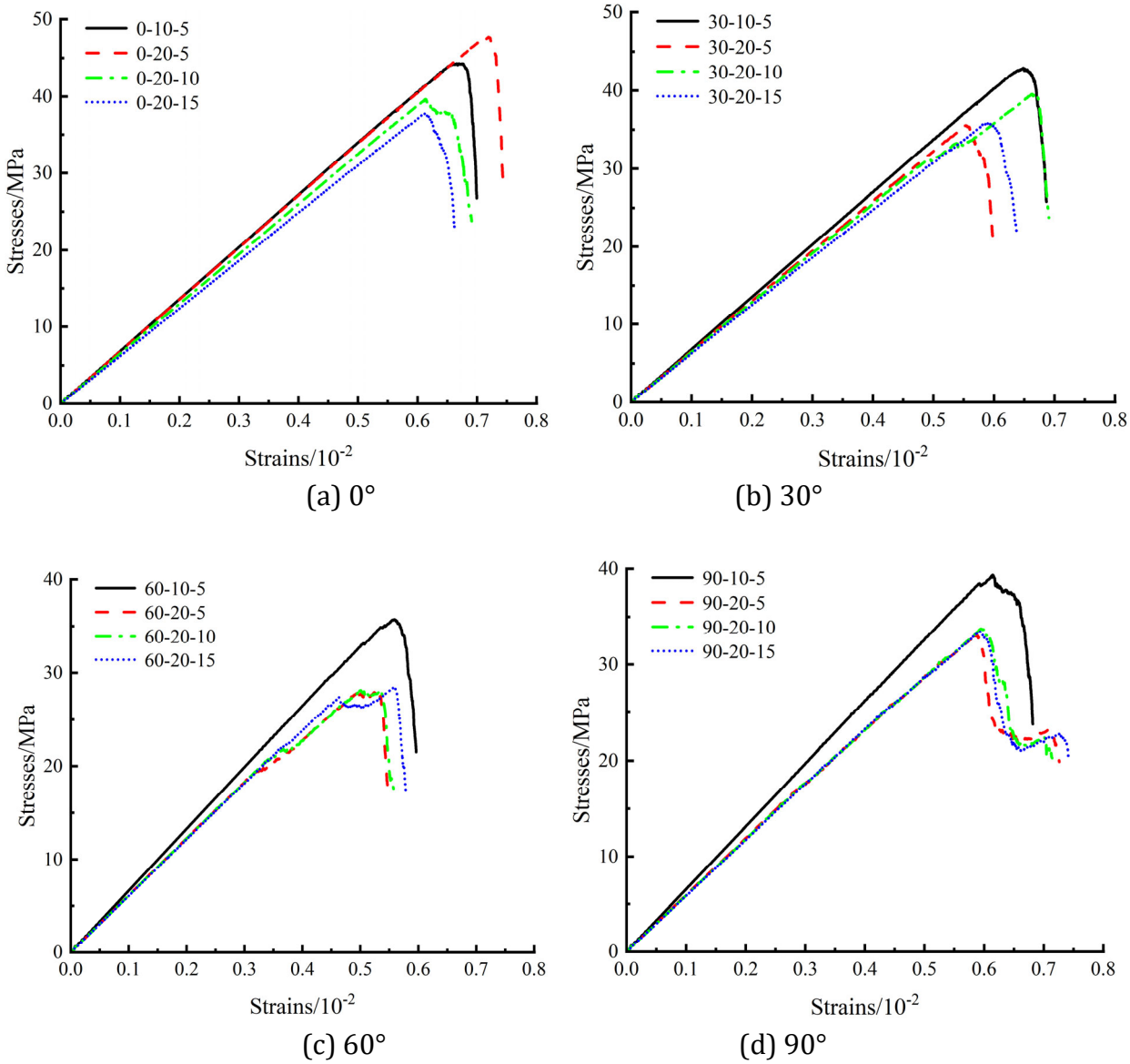

Figure 6. Stress-strain curves for different fissure lengths

To observe the variation trend of peak stress and peak strain with changes in fracture length more clearly, the peak stress and peak strain under different fracture lengths from Figure 6 are plotted in Figure 7. From Figure 7(a), it can be seen that when the length of the secondary fracture remains constant, the peak stress of the specimen with a 0° fracture angle increases with the increase in the length of the main fracture, while for specimens with fracture angles of 30° to 90°, the peak stress decreases as the main fracture length increases. When the length of the main fracture remains constant, the peak stress of the specimen with a 0° fracture angle decreases with the increase in the length of the secondary fracture. The peak stress of the 30° specimen increases initially and then decreases with the length of the secondary fracture, while for 60° to 90° specimens, the peak stress remains relatively unchanged as the length of the secondary fracture increases. Figure 7(b) shows that when the length of the secondary fracture is constant, only the peak strain of the 0° specimen increases with the increase in the length of the main fracture, whereas the peak strain of specimens with 30° to 90° fracture angles decreases with an increase in the main fracture length, with the 30° specimen showing the largest reduction. When the main fracture length remains constant, the peak strain of the 0° specimen decreases with an increase in the length of the secondary fracture, while the peak strain of the 30° specimen first increases and then decreases with the length of the secondary

ISSN: 2710-0588

fracture. The peak strain of the 60° specimen first decreases and then increases with the length of the secondary fracture, while the peak strain of the 90° specimen remains relatively steady with the increase in the secondary fracture length.

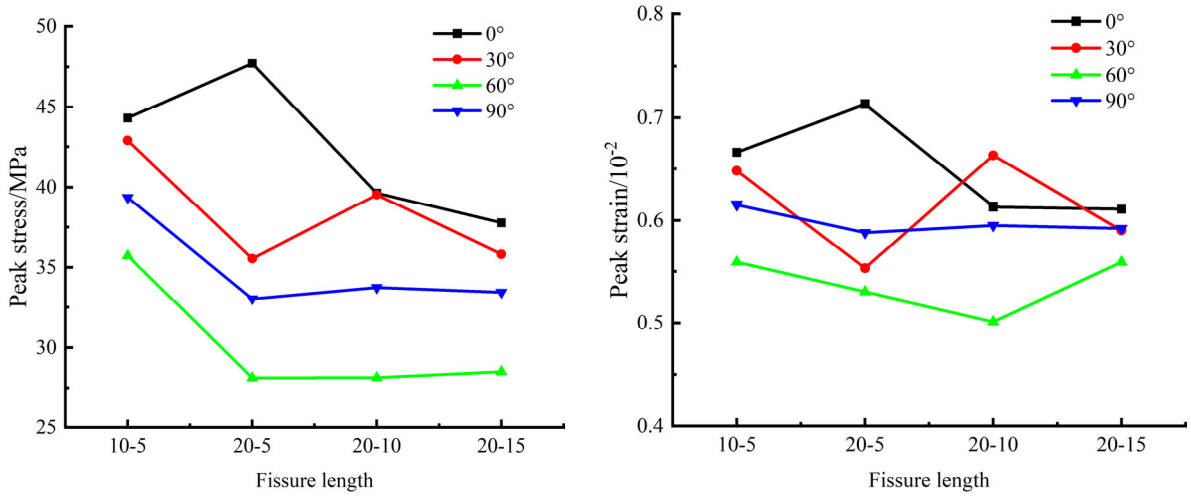

(a) Peak stress (b) Peak strain

Figure 7. Peak stress, peak strain variation curve with fissure lengths

4. The Propagation and Evolution Law of Cracks

4.1. Crack initiation location

The initiation of cracking positions for each specimen during the uniaxial compression process is illustrated in Figure 8. From Figure 8, it is evident that for the specimen with a crack inclination of 0°, when the secondary crack length is 5mm, the initiation of cracking does not occur at the tip of the pre-existing crack but rather around it. When the secondary crack length increases to 10mm, the initiation point begins to appear at the tip of the main crack. For specimens with crack inclinations of 30° to 60°, the initiation of cracking is consistently located at the tip of the main crack, and as the secondary crack length increases, the initiation position also begins to appear at its tip. A comparison of the specimens with crack inclinations of 0° and 90° reveals that both the crack length and inclination significantly affect the initiation position. At a crack inclination of 0°, as the secondary crack length increases, the initiation position gradually shifts from around the crack to the tip of the main crack; at a crack inclination of 90°, the initiation positions are consistently located at the tip of the secondary crack. When both the vertical length of the crack relative to the main stress direction and the horizontal length parallel to it are substantial, the initiation position will emerge at the tip of the crack aligned with the main stress direction. Conversely, when the vertical crack length is greater than the horizontal crack length, the initiation position will always occur at the tip of the crack parallel to the main stress direction. When there is a certain angle between the primary and secondary crack directions and the main stress direction, the initiation of cracking preferentially occurs at the tip of the main crack. As the secondary crack length increases, the initiation position also starts to appear at the tip of the secondary crack, generally expanding in the same direction as the loading.

ISSN: 2710-0588

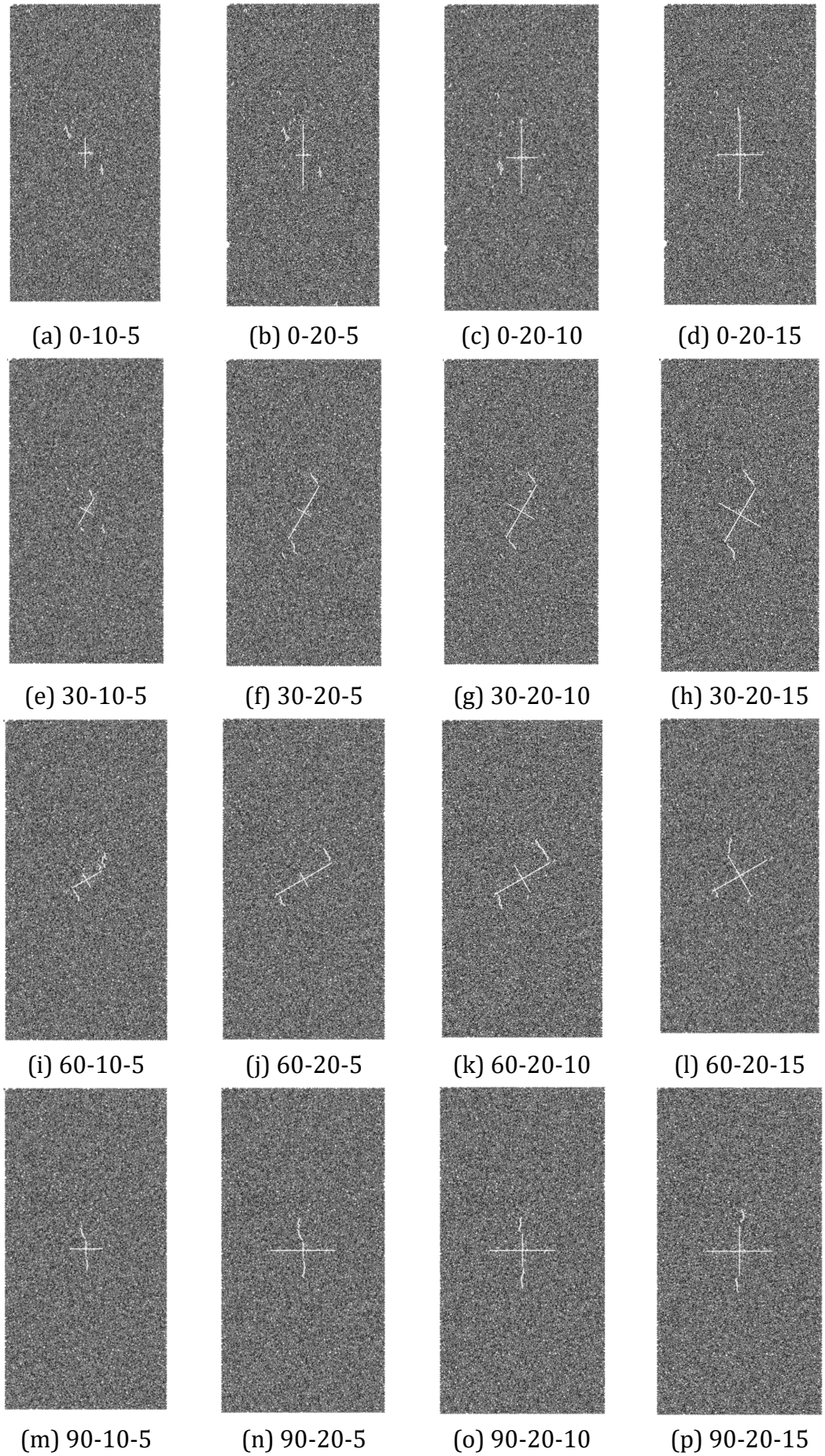

(a) 0-10-5 (b) 0-20-5 (c) 0-20-10 (d) 0-20-15

(e) 30-10-5 (f) 30-20-5 (g) 30-20-10 (h) 30-20-15

(i) 60-10-5 (j) 60-20-5 (k) 60-20-10 (l) 60-20-15

(m) 90-10-5 (n) 90-20-5 (o) 90-20-10 (p) 90-20-15

Figure 8. Location of crack initiation

ISSN: 2710-0588

4.2. Mesoscopic damage evolution process

The evolution of micro-damage for several specimens with different crack inclinations and lengths during loading is shown in Table 3. An analysis of three characteristic points during the compression process (I, II, III) was conducted, where I represents the early stage of loading, II represents the initiation position, and III denotes the peak stress. The evolution of force chains and crack classifications at different characteristic points is discussed. In the force chain diagram, blue represents compression links, green represents tension links, while in the crack classification diagram, red represents tensile cracks, and black represents shear cracks.

Table 3. Microscopic damage evolution process

number	type	I	II	III
0-10-5	Contact force chain	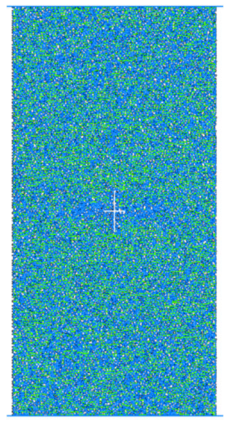	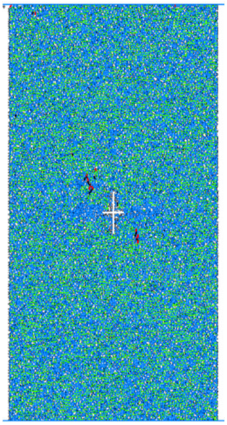	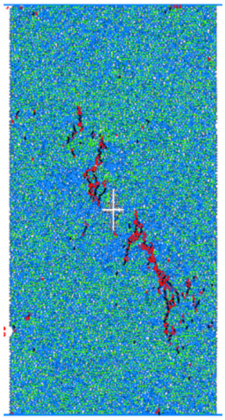
	Fracture classification		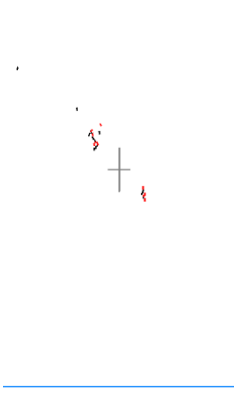	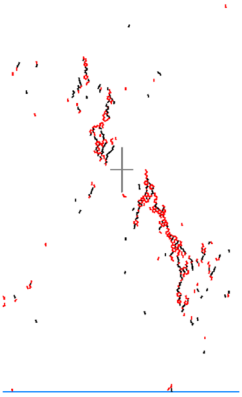
0-20-5	Contact force chain	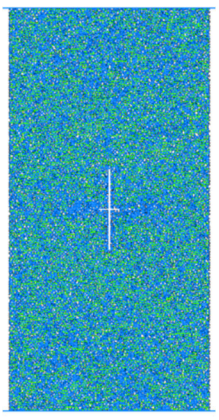	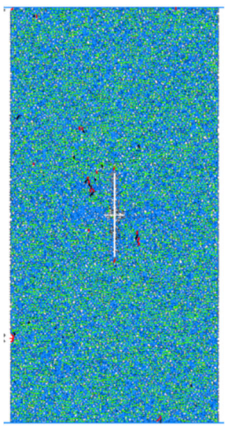	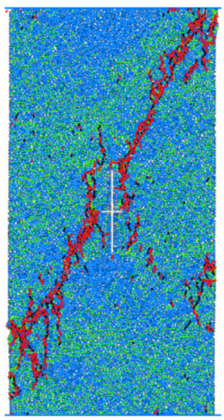

ISSN: 2710-0588

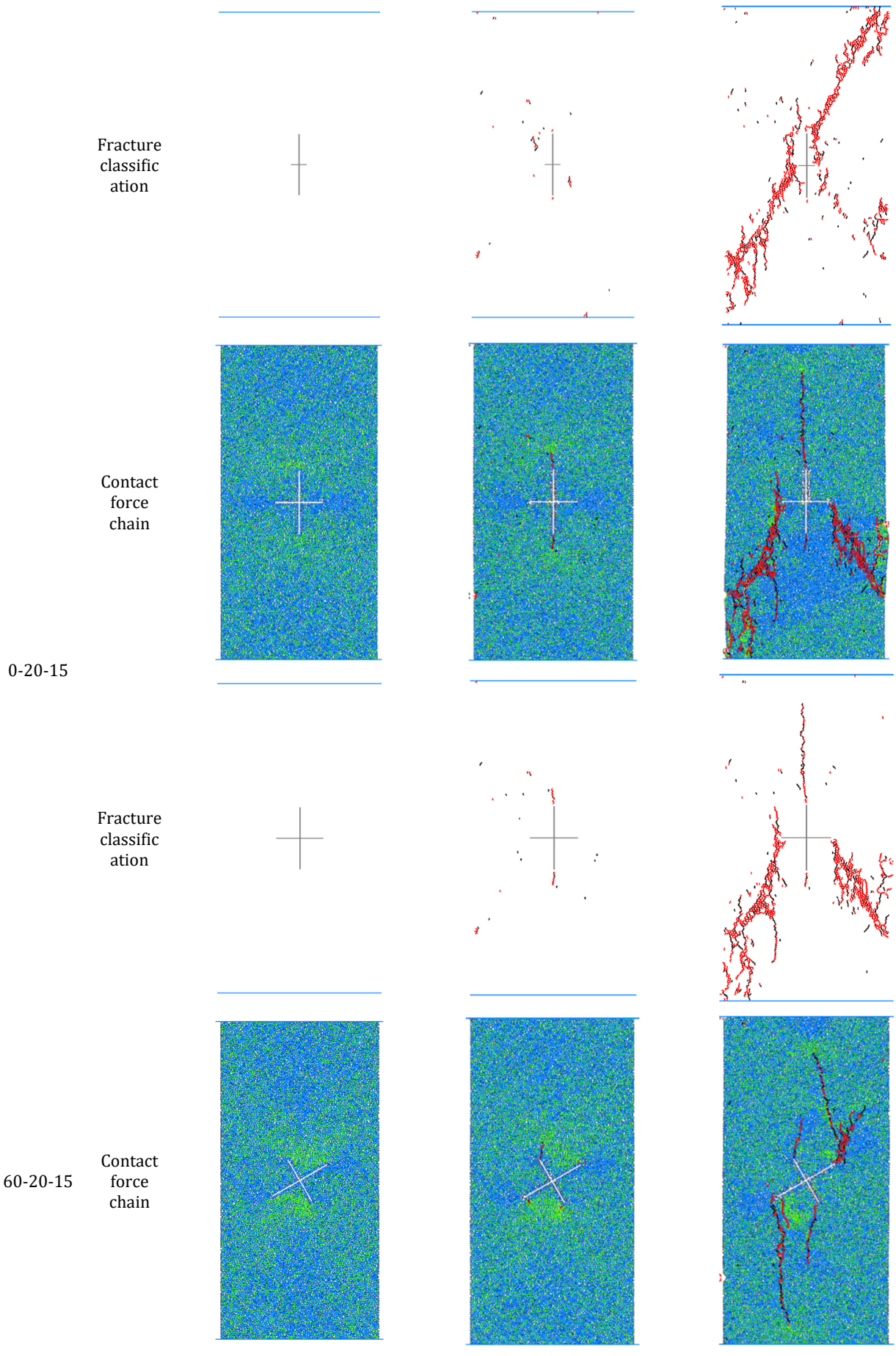

ISSN: 2710-0588

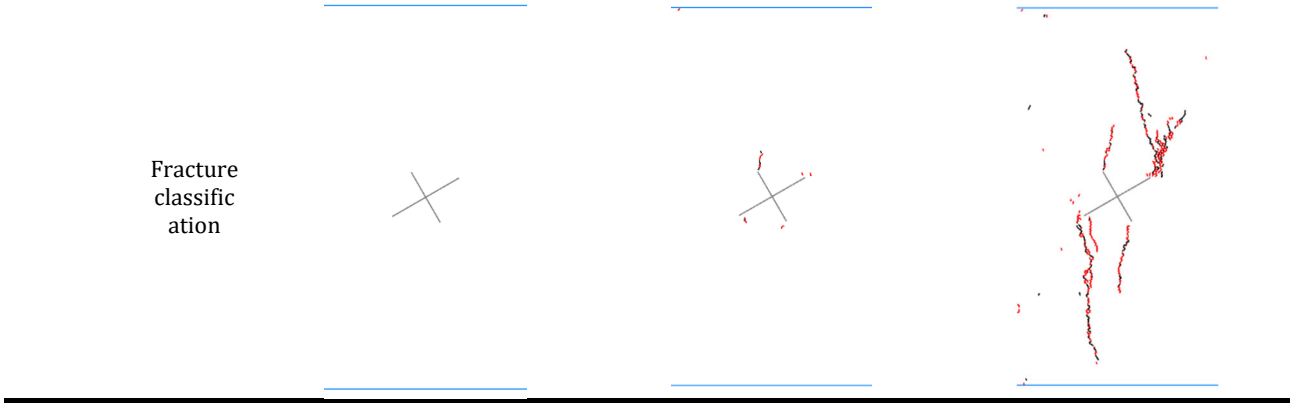

At the early loading stage (I), the internal blue compression force chains in the specimen extend mainly along the loading direction, while the green tension force chains extend primarily in the horizontal direction. For the specimen with a crack inclination of 0°, significant blue compressive stress concentration is observed at both ends of the secondary crack, and the increase in the main crack does not lead to substantial changes in the distribution of force chains. However, the increase in the secondary crack length results in a noticeable concentration of green tensile stress at both ends of the main crack. For the specimen with a crack inclination of 60°, the green tensile stress concentration appears between the main and secondary cracks, with blue tensile stress concentrated at the tip of the crack. During this stage, the forces within the specimen are all below the bearing capacity of the force keys, and the force keys do not fracture, hence no micro-cracks are formed.

At the initiation position (II), the distribution of contact force keys within the specimen does not show significant changes, with concentrated stresses still distributed at both ends of the cracks and between the cracks. At this point, some maximum contact forces begin to exceed the strength of the force keys, causing them to fracture. For the specimens 0-10-5 and 0-20-5, micro-cracks first appear around the pre-existing cracks; for the specimens 0-20-15 and 60-20-15, micro-cracks first appear at the tip of the pre-existing cracks, generally extending along the loading direction.

At peak stress (III), distinct partitioning appears in the particle contact network within the specimen, with stress concentrations at the tip of the pre-existing cracks. Micro-cracks extend along the loading direction and quickly penetrate, forming a macroscopic fracture zone. Red tensile cracks and black shear cracks intertwine, with a significant proportion of the cracks being red tensile cracks.

4.3. Final failure mode

The final failure modes of each specimen are shown in Figure 9. From Figure 9, it can be seen that for the specimen with a crack inclination of 0°, when the secondary crack length remains unchanged, an increase in the main crack length results in a change in the crack propagation mode, displaying a relatively classic diagonal failure pattern, with cracks originating around the crack and propagating towards the ends. When the main crack length remains unchanged, as the secondary crack length increases, the final failure mode of the specimen gradually shifts from being dominated by the secondary crack to a "figure-eight" shape, with cracks originating at the tip of the secondary crack extending downward and penetrating, while cracks formed at the tip of the main crack do not penetrate. For specimens with crack inclinations of 30° and 60°, when the secondary crack is relatively short, failure is dominated by the main crack, with cracks originating at the tip of the main crack extending towards both ends and penetrating. As the main crack length increases, the position of penetration during specimen failure gradually lowers from the corners of the specimen, with the propagation direction generally aligning with

ISSN: 2710-0588

the main stress direction. When the main crack length remains unchanged, as the secondary crack length increases, the specimen with a crack inclination of 30° gradually transitions to a mode where cracks originating at the tip of the secondary crack extend downward and penetrate, while cracks originating at the tip of the main crack do not penetrate. For the specimen with a crack inclination of 60°, failure remains controlled by the main crack, although the extension length of cracks formed at the tip of the secondary crack gradually increases. In the case of the specimen with a crack inclination of 90°, cracks always extend downward and penetrate from the tip of the main crack, while cracks originating at the tip of the secondary crack do not penetrate.

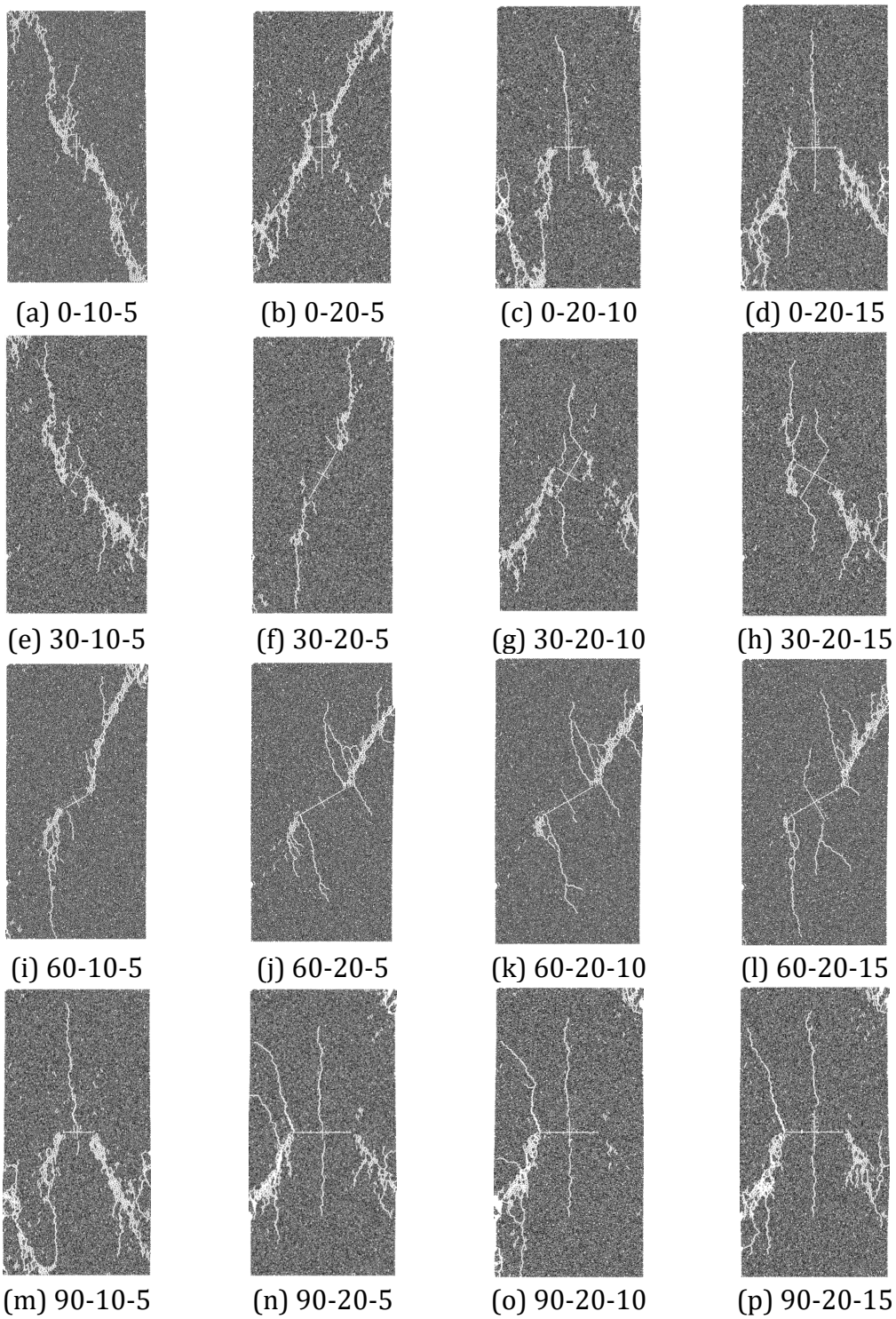

Figure 9. Final destructive form

ISSN: 2710-0588

5. Conclusion

(1) The peak stress and peak strain of sandstone orthogonal fissure samples decrease and then increase with the increase of inclination angle, reaching a minimum at 60°. Among these, the 20-5 sample within the range of 0°-30° is the most sensitive to changes in angle, showing a peak stress reduction of 25.50%. In the range of 30°-60°, the 20-10 sample displays the largest peak stress reduction (28.83%), and the overall reduction in peak stress in this interval is greater than that in the 0°-30° range. From 60°-90°, all samples exhibit a gradual increase in both peak stress and peak strain.

(2) As the length of the main fissure increases, the peak stress and peak strain of the 0° inclination sample increase, while those of the 30°-90° inclination samples show a decreasing trend. When the length of the secondary fissure increases, the peak stress and peak strain of the 0° inclination sample decrease, the 30° inclination sample initially increases and then decreases, and the peak stress and peak strain of the 60°-90° inclination samples remain relatively stable.

(3) At 0° inclination, the growth of secondary fissures causes the crack initiation point to shift from the intersection to the tip of the main fissure, with the failure mode transitioning from diagonal failure to a "figure-eight" pattern of penetration. Between 30°-60°, the main fissure initiates and dominates the failure process. At 90°, although the secondary fissures initially develop, they ultimately lead to a "figure-eight" pattern of failure characterized by the penetration of the main fissure. The samples primarily exhibit tensile failure, with cracks originating from pre-existing fissures and extending outward along the direction of the principal stress towards both ends.

References

[1] Yang S, Yin P, Zhang Y, et al. Failure behavior and crack evolution mechanism of a non-persistent jointed rock mass containing a circular hole[J]. International Journal of Rock Mechanics and Mining Sciences,2019,114101-121.

[2] Huimei Z, Chao Y, Shiguan C, et al. Experimental study of fracture geometry characteristics on rock mass strength and crack propagation evolution law[J]. European Journal of Environmental and Civil Engineering,2022,26(16):7972-8001.

[3] Li C, Pan L, Zhang L, et al. Deformation localization and crack propagation of sandstone containing different flaw inclination angles under different loading rates[J]. Frontiers in Earth Science,2023,11

[4] Guangfeng L, Quansheng L, Xingxin P, et al. Experimental study on mechanical properties of fractured rock mass under different anchoring modes[J]. European Journal of Environmental and Civil Engineering,2020,24(7):931-948.

[5] Haeri H, Shahriar K, Marji F M, et al. On the strength and crack propagation process of the pre-cracked rock-like specimens under uniaxial compression[J]. Strength of Materials,2014,46(1):140-152.

[6] Ma W, Ma Y. A synthetic study of cracking behavior and fracture mechanism of sandstone containing two non-connected fissures under uniaxial compression[J]. Computational Particle Mechanics, 2024, 12(2):1-23.

[7] Du X, Liu W, Huang B. Experimental and Simulation Studies on the Effect of Rock Bridges on Rock Failure[J]. Geotechnical and Geological Engineering,2024, 1-14.

[8] Peng C, Du X, Li Z, et al. Experimental and simulation study on compressive failure of rock with pre-Y-shaped cracks[J]. PloS one,2024,19(11):e0312344.

[9] Lin H, Li S, Zhang X. Macro-micro failure and crack coalescence behavior of soft-hard composite rock with three parallel joints under uniaxial compression[J]. Journal of Materials Research and Technology,2024,292947-2958.

ISSN: 2710-0588

[10] Qingzhi C, Yuanming L, Wei W, et al. Effects of Normal Stress and Joint Inclination Angle on Rock Failure Characteristics Under Compression–Shear Conditions[J]. Frontiers in Earth Science,2022,10.

[11] Castro-Filgueira U, Alejano R L, Ivars M D. Particle flow code simulation of intact and fissured granitic rock samples[J]. Journal of Rock Mechanics and Geotechnical Engineering,2020,12(5):960-974.

[12] Zhao C, Niu J, Zhang Q, et al. Numerical Simulations on Cracking Behavior of Rock-Like Specimens with Single Flaws under Conditions of Uniaxial and Biaxial Compressions[J]. Journal of Materials in Civil Engineering,2019,31(12):04019305-04019305.

[13] Lee H, Jeon S. An experimental and numerical study of fracture coalescence in pre-cracked specimens under uniaxial compression[J]. International Journal of Solids and Structures, 2010, 48(6): 979-999.

[14] Bahaaddini M, Sharrock G, Hebblewhite B. Numerical investigation of the effect of joint geometrical parameters on the mechanical properties of a non-persistent jointed rock mass under uniaxial compression[J]. Computers and Geotechnics,2013,49206-225.

[15] Fan X, Kulatilake P, Chen X. Mechanical behavior of rock-like jointed blocks with multi-non-persistent joints under uniaxial loading: A particle mechanics approach[J]. Engineering Geology, 2015, 19017-32.

[16] Wu J, Chen Z, Feng M, et al. The length of pre-existing fissure effects on the dilatancy behavior, acoustic emission, and strength characteristics of cracked sandstone under different confining pressures[J]. Environmental Earth Sciences,2018,77(12):1-14.

[17] Feng P, Dai F, Liu Y, et al. Effects of strain rate on the mechanical and fracturing behaviors of rock-like specimens containing two unparallel fissures under uniaxial compression[J]. Soil Dynamics and Earthquake Engineering,2018,110195-211.

[18] Yang X, Kulatilake P, Jing H, et al. Numerical simulation of a jointed rock block mechanical behavior adjacent to an underground excavation and comparison with physical model test results[J]. Tunnelling and Underground Space Technology incorporating Trenchless Technology Research, 2015, 50129-142.